NUMERICAL SIMULATION OF POROUS BURNERS AND HOLE PLATE SURFACE BURNERS

by

Stevan NEMODA, Dimosthenis TRIMIS, and Goran ŽIVKOVIĆ

Original scientific paper
UDC: 662.951.2:532.546:519.876.5
BIBLID: 0354–9836, *8* (2004), 1, 3-17

In comparison to the free flame burners the porous medium burners, especially those with flame stabilization within the porous material, are characterized by a reduction of the combustion zone temperatures and high combustion efficiency, so that emissions of pollutants are minimized. In the paper the finite-volume numerical tool for calculations of the non-isothermal laminar steady-state flow, with chemical reactions in laminar gas flow as well as within porous media is presented. For the porous regions the momentum and energy equations have appropriate corrections. In the momentum equations for the porous region an additional pressure drop has to be considered, which depends on the properties of the porous medium. For the heat transfer within the porous matrix description a heterogeneous model is considered. It treats the solid and gas phase separately, but the phases are coupled via a convective heat exchange term. For the modeling of the reaction of the methane laminar combustion the chemical reaction scheme with 164 reactions and 20 chemical species was used. The proposed numerical tool is applied for the analyses of the combustion and heat transfer processes which take place in porous and surface burners. The numerical experiments are accomplished for different powers of the porous and surface burners, as well as for different heat conductivity characteristics of the porous regions.

Key words: *gas combustion, numerical simulation, porous medium burners*

Introduction

In recent years, new and improved burner concepts, especially for gaseous fuels, have been developed. Main task of the new generation of gaseous burners is to provide the basis for low NO_x and CO emission combustion systems. In comparison to free flame burners, the porous medium burners, especially those with flame stabilization within the porous material, allow the combustion zone temperatures control, so that the emissions of

pollutants are minimized. Furthermore, the porous medium combustion technology is characterized by higher burning rates and increased flame stability. On account of these qualities, there are diverse fields of application for porous media combustion, such as water or air heaters for industrial and domestic applications. In order to optimize the combustion processes in porous media, to make them high efficient, to obtain low emissions of pollutants, and to rapidly adapt porous materials and burner geometries to new applications, numerical codes are necessary.

The adapted version of the finite-volume CFD-code FASTEST-2D was used for the calculations of the non-isothermal laminar steady-state flow, with chemical reactions within the porous media. For the evaluation of the convective and diffusive heat and mass transfer, the energy equation and the conservation equations for the relevant species of the gas mixture were solved. For the porous regions the momentum and energy equations have appropriate corrections. In addition, for more detailed numerical simulation of heat transport processes within the porous region, the so-called heterogeneous heat transfer model is applied. The model describes separately gas and solid phase heat transfer, as well as heat transfer between gas and solid matrix. The radiation heat transfer within the porous matrix was included in the effective heat conductivity coefficients of the porous medium. The process of gaseous fuel combustion was described by chemical kinetics for the relevant species, and by the modeling of the source term which represents the reaction rate.

The primary aim of the present paper is to show a proposed concept of the numerical simulation of complex processes in the porous burners. Besides, the proposed numerical tool is applied for the analyses of the combustion and heat transfer processes which take place in porous and surface burners. The numerical experiments are accomplished for different powers of the porous and surface burners, as well as for different heat conductivity characteristics of the porous regions.

Numerical description

Neglecting the forced turbulent effects within pores, for the description of the porous media combustion processes the laminar flow effects are adopted. Thus, the equations for laminar, nonisothermal, steady flow of a chemically reacting mixture of Newtonian, perfect gases are considered. The basic conservation equations in tensor notation governing the transport of, momentum, energy and mass are:

Continuity equation:

$$\frac{\partial}{\partial x_j}(\rho U_j) \quad 0 \tag{1}$$

Momentum equation in *i* direction:

$$\frac{\partial}{\partial x_j}(\rho U_j U_i) \quad \frac{\partial}{\partial x_j} \quad \mu \frac{\partial U_i}{\partial x_j} \qquad \frac{\partial p}{\partial x_i} \quad \frac{\partial}{\partial x_j} \quad \mu \frac{\partial U_j}{\partial x_i} \quad \frac{2}{3} \frac{\partial}{\partial x_i} \quad \mu \frac{\partial U_k}{\partial x_k} \tag{2}$$

Energy equation:

$$\frac{\partial}{\partial x_j}(\rho U_j h) \quad \frac{\partial}{\partial x_j} \frac{\lambda}{c_p} \frac{\partial h}{\partial x_j} \quad \sum_{k\ 1}^{N_s} R_k H_k \quad \frac{\partial}{\partial x_j} \sum_{k\ 1}^{N_s} \rho D_k h_k \frac{\partial Y_k}{\partial x_j} \quad Q_R \qquad (3)$$

Mass transfer equation:

$$\frac{\partial}{\partial x_j}(\rho U_j Y_k) \quad \frac{\partial}{\partial x_j} \rho D_k \frac{\partial Y_k}{\partial x_j} \quad R_k \qquad (4)$$

The dynamic viscosity μ, heat conductivity λ, and mass diffusion coefficient D_k for a mixture of N_S species are calculated from the properties of the pure species using semi-empirical approximations. The properties of the pure species are estimated from the kinetic gas theory. The heat capacity c_p and other thermodynamic data, including the heat of formation H_k were obtained from the CHEMKIN II thermodynamic property database [3]. The production and conversion of species k due to the chemical reactions enter as a source/sink term R_k in the transport equations of species. Taking into account that only laminar combustion processes are assumed, R_k can be defined by:

$$R_k \quad M_k \sum_{l\ 1}^{N_R} (\nu_{kl} \quad \nu_{kl}) k_l \prod_{\text{educts}} c^{\nu_{kl}} \quad \frac{1}{K_C} \prod_{\text{products}} c^{\nu_{kl}} \qquad (5)$$

where N_R is the number of reactions l. For each of chemical reactions l the balance of atom species A_k must be satisfied:

$$\sum_{k\ 1}^{N_s} \nu_{kl} A_k \quad \sum_{k\ 1}^{N_s} \nu_{kl} A_k \qquad (6)$$

The reaction rate constants k_l are determined by the Arrhenius expression:

$$k_l \quad k_l^0 T^a \exp \quad \frac{E_l}{RT} \qquad (7)$$

The last two terms of eq. (3) correspond to the energy flux term caused by the diffusion of components in multicomponent systems and to radiation source term given in a general form.

Modelling of flow and heat transfer effects in porous media

A porous media consists of solid and fluid phases. Models that resolve the pore structure in detail are very complex and are not applicable for practical applications. Therefore, the porous medium is commonly considered as pseudo-homogeneous (locally volume-averaged) medium, wherein the solid and the fluid phases are treated as an artificial unique phase. Within the scope of the presented calculations a heterogeneous model is

considered for the heat transfer description. It treats the solid and gas phase separately, but the phases are coupled via a convective heat exchange term. The heterogeneous model enables more detailed description of heat transfer processes, what is especially important for high porous matrix such are combustion zones in the porous burners.

With these assumptions the governing equations for the pseudo-homogeneous porous media, including the heterogeneous heat transfer model, have a similar form, with the certain corrections, to those of a single-phase flow, eq. (1-4).

In all equations the fluid velocity is replaced by the superficial velocity based on the area of the empty tube.

In the momentum equations an additional pressure drop has to be considered, which depends on the properties of the porous medium. Second order polynomials are used to describe this pressure drop according to the Forchheimer equation for the *i*-th direction.

$$\frac{\partial p}{\partial x_i} \quad \frac{\mu}{K_{1,i}} U_j \quad \frac{\rho}{K_{2,i}} U_j \left| U_j \right| \tag{8}$$

where U_j is the superficial velocity based on the sectional area of the empty tube. The tensors $K_{1,i}$ and $K_{2,i}$ are the linear and turbulent permeability coefficients that describe the pressure loss in the porous medium. These coefficients can be experimentally determined.

The heat transfer model, according to the heterogeneous approach for the porous regions consists of two equations, for gas and solid phase:

Gas phase:

$$\begin{aligned} &\frac{\partial}{\partial x_j}(\rho U_j c_p T_g) \quad \frac{\partial}{\partial x_j} \quad \frac{\varepsilon \lambda_g}{c_p} \frac{\partial (c_p T_g)}{\partial x_j} \\ &\varepsilon \sum_{k\ 1}^{N_s} R_k H_k \quad \frac{\partial}{\partial x_j} \sum_{k\ 1}^{N_s} \rho D_k \varepsilon (c_{p,k} T)_g \frac{\partial Y_k}{\partial x_j} \quad \alpha A_V (T_s \quad T_g) \end{aligned} \tag{9}$$

Solid phase:

$$\frac{\partial}{\partial x_j} \ (1 \quad \varepsilon) \lambda_{\text{eff}} \frac{\partial T_s}{\partial x_j} \quad \alpha A_V (T_s \quad T_g) \quad Q_R \tag{10}$$

where ε is the porosity, α is the gas-solid heat transfer coefficient, A_V is the porous matrix specific surface, T_s is the solid temperature, λ_g is the gas conductivity, λ_{eff} is the effective conductivity of the porous region and Q_R is the radiation heat transfer between solid and environment.

The changes for the mass transfer equation are also necessary:

$$\frac{\partial}{\partial x_j}(\rho U_j Y_k) \quad \frac{\partial}{\partial x_j} \ \varepsilon \rho D_k \frac{\partial Y_k}{\partial x_j} \quad \varepsilon R_k \tag{11}$$

The radiation heat transfer is modeled by eq. (10) separately for heat transfer within porous matrix (by λ_{eff}) and between the solid phase and the environment, Q_R.

The effective heat transfer coefficient λ_{eff} includes all major mechanisms of energy transport in porous media and depends on the heat conductivities of the solid and the fluid phase, the radiation properties of both phases, the pressure, the temperature and the porosity and geometry of the porous matrix (characteristic pore diameter, pore shape, *etc*.). In addition, it is also a function of the flow because convective dispersion effects are superposed. This leads to an anisotropic formulation of the heat conductivity, which reads for the *i* direction:

$$\lambda_{\text{eff}_i} \quad \lambda^0_{\text{eff}} \quad \frac{\frac{\dot{m}}{A} c_p d}{k_i} \tag{12}$$

The heat conductivity is divided in two parts: one for the effective heat conductivity without flow (λ^0_{eff}) and one for the convective dispersion effects. The second part depends on the mass flow density ($\dot{m}/A$), the heat capacity of the fluid c_p, a characteristic diameter (the pores hydraulic diameter) d, and the dispersion coefficients k_i.

The radiation heat transfer between the solid phase and the environment can be defined using the extinction formulation for the porous matrix:

$$Q_{R,i} \quad (1 \quad \varepsilon) \frac{a \mathrm{C}_{\mathrm{B}} (T^4 \quad T_0^4)}{\Delta l} \mathrm{e}^{\ \psi x} \quad \psi \quad \frac{1}{\Delta l} \ln \varepsilon \tag{13}$$

where Δl is the characteristic length which is proportional to the hydraulic diameter of the pores and can be used as a model constant, ψ is the extinction coefficient for the porous matrix, a is the emissivity, and $\mathrm{C_B}$ is the Stefan-Boltzmann constant ($5.67 \cdot 10^{-8}$ $\mathrm{W/m^2K^4}$).

Numerical method

Each equation from the given system of equations can be formulated in a general elliptical transport equation form:

$$\frac{\partial}{\partial x_j}(\rho U_j \phi) \quad \frac{\partial}{\partial x_j} \quad \Gamma_\phi \frac{\partial \phi}{\partial x_j} \quad S_\phi \tag{14}$$

where ϕ is the general transported variable, Γ_ϕ is the corresponding effective diffusion coefficient, and S_ϕ are sources and sinks of ϕ. The terms on the left side of eq. (14) correspond to the convective and diffusion processes respectively, and a term on the right side represents source/sink in the transport equation of the variable ϕ.

The finite volume method is applied for the spatial discretisation and the variable arrangement is collocated. The basic procedure for the formulation is adapted for the two-dimensional flow with porous regions. The solution domain was discretised by a

structured non-orthogonal, blocked grid. The resulting system of algebraic equations was solved through the semi-implicit procedure according to 1 . Pressure and velocity were coupled by the SIMPLE algorithm 2 .

Problem formulations

The considered cases are shown schematically in fig. 1. Basically two cases are analyzed: porous burner with two porous regions (Case 1) and surface burner with only one porous region (flame stabilization) (Case 2). Both cases consider rectangular burners with two different regions. First region is a preheating region (Zone A) which consists of porous matrix with small pores (ε = 10%) followed by the actual combustion region (Zone C) which is, in case of the porous burner, porous matrix with larger pores (ε = 90%) and in case of the surface burner it is the gas region. After ignition, combustion is self-stabilized at the interface between these two regions. The preheating region A of the studied burner is composed of aluminum oxide (Al_2O_3) hole plate and the combustion region C is made of a SiC foam.

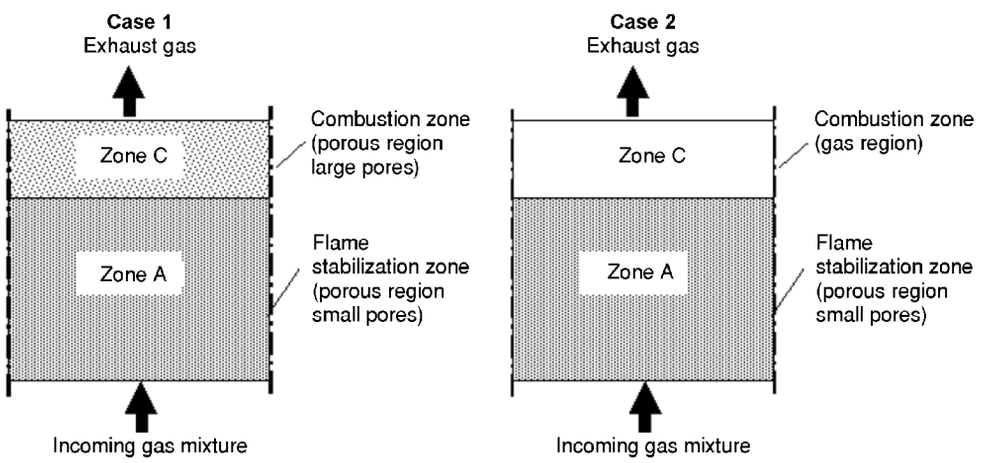

Figure 1. Cases for numerical experiments

The numerical experiments for both cases were done for three different power densities (for Case 1: 350, 1000, and 2000 kW/m^2; for Case 2: 100, 200, and 300 kW/m^2). Moreover, for each power the calculations with three different effective heat conductivities of the porous region A were completed. The effective heat conductivities were artificially defined, but taking into account real dependences of the velocity and temperature of Al_2O_3 hole plate (Zone A) and SiC porous matrixes (Zone C), eq. (12).

The porous matrix effective heat conductivities without flow (λ^0_{eff}) were defined by polynomial temperature dependences based on experiments 4 . The convective dispersion effects were calculated by eq. (12) using experimentally obtained values of the dispersion coefficients 4 . In fig. 2 the effective heat conductivities of regions A (Al_2O_3 hole plates) in function of temperature are shown. Regarding the determination of the solid-gas heat transfer properties are concerned: for Al_2O_3 hole plates (Zone A) it is possible to calculate α and A_V; and for SiC foam (Zone C) the semi-empirical dependence $A_V = f(\text{Re}, \lambda_g)$ is used from 5 .

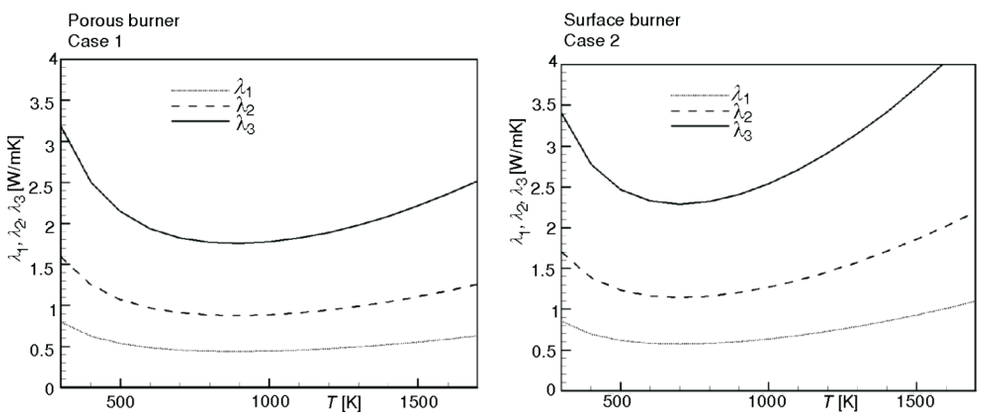

Figure 2. Effective heat conductivities of the Zone A in function of temperature

For all calculations the presented model, eqs. (1-13) was used. The equations of the model are two-dimensional, but due to the symmetrical boundary conditions on lateral sides of the calculation regions (fig. 1) there were neglected gradients of the analyzed variables. It has been already mentioned that all model equations can be reduced to general form, eq. (14). Therefore, all model equations used for the analyzed numerical experiments, are defined by eq. (14) and tab. 1. It comprises transport variables, diffusion coefficients and source/sink terms for all model equations.

All calculations were performed with the same boundary conditions. For all calculations the air-methane burning mixture has been taken, whereby air excess ratio was 1.2. Since all numerical experiments were performed with same geometry (fig. 1), power was changed by varying the incoming gas mixture velocity (with temperature of 293 K).

For modeling the reaction of the methane combustion the chemical reaction scheme with 164 reactions and 20 chemical species was used 6 .

Presented numerical experiments were primarily performed to test the proposed numerical tool by comparing the combustion characteristics in a porous burner and in a surface burner, as well as by analyzing the power density and the porous matrix heat conductivity influences on combustion properties.

Table 1. Model equations transport variables, diffusion coefficients, and source/sink terms

Equation	Dependent variable, ϕ	Coefficient, Γ_{eff}	Source term, S_ϕ
Continuity	1	0	0
Momentum in x_i direction	U_i	μ	$\frac{\partial}{\partial x_j}\ \mu\frac{\partial U_j}{\partial x_i}\quad\frac{\partial p}{\partial x_i}$
Momentum in x_i direction for porous region	U_i	μ	$\frac{\partial}{\partial x_j}\ \mu\frac{\partial U_j}{\partial x_i}\quad\frac{\partial p}{\partial x_i}\quad\frac{\mu}{K_{1,j}}U_j\quad\frac{\rho}{K_{2,j}}U_j\lvert U_j\rvert$
Energy of gas out of porous matrix	c_pT_g	λ_g/c_p	$\sum_{k\ 1}^{N_s}R_kH_k\quad\frac{\partial}{\partial x_j}\ \sum_{k\ 1}^{N_s}\rho D_k h_k\frac{\partial Y_k}{\partial x_j}$
Energy for gas phase within porous matrix	c_pT_g	$\varepsilon\lambda_g/c_p$	$\varepsilon\sum_{k\ 1}^{N_s}R_kH_k\quad\frac{\partial}{\partial x_j}\ \sum_{k\ 1}^{N_s}\rho D_k\varepsilon\,(c_{p,k}T)_g\frac{\partial Y_k}{\partial x_j}$ $\alpha A_V(T_s\quad T_g)$
Energy for solid phase	for convec. term: 0 for diffusion term: T_s	$(1-\varepsilon)\lambda_{\text{eff}}$	$\alpha A_V(T_s\quad T_g)\quad Q_R$
Species transport for gas region	Y_k	ρD_k	R_k
Species transport for porous region	Y_k	$\varepsilon\rho D_k$	εR_k

Results

All calculations were performed in the two-dimensional geometry, but because of symmetry boundary conditions on lateral sides of the calculation regions (fig. 1) there were neglecting gradients of the analyzed variables. Therefore the presented results are always extracted profiles in the axial direction (flow direction).

The calculated porous burner (Case 1) temperature profiles for the solid and the gas phase at a power densities of 350, 1000, and 2000 kW/m^2 are shown in figs. 3-7. Each figure shows the calculations with three different effective heat conductivities of the porous region A: λ_1 – low heat conductivity, λ_2 – medium heat conductivity, and λ_3 – high heat

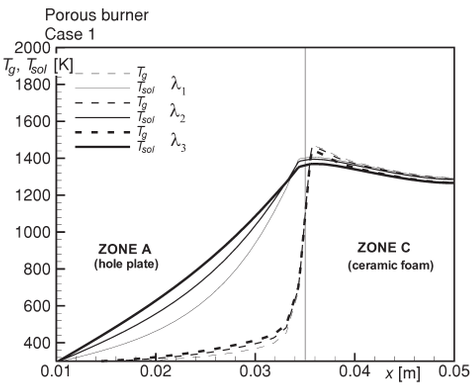

Figure 3. Temperature profiles at power density of 350 kW/m^2

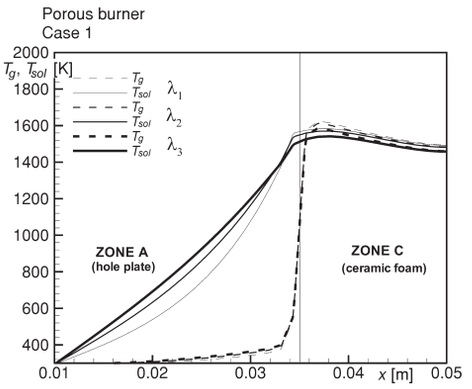

Figure 4. Temperature profiles at power density of 1000 kW/m^2

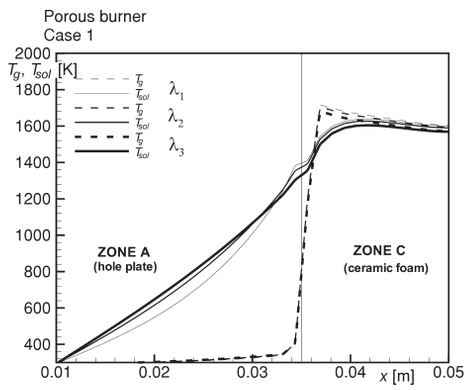

Figure 5. Temperature profiles at power density of 2000 kW/m^2

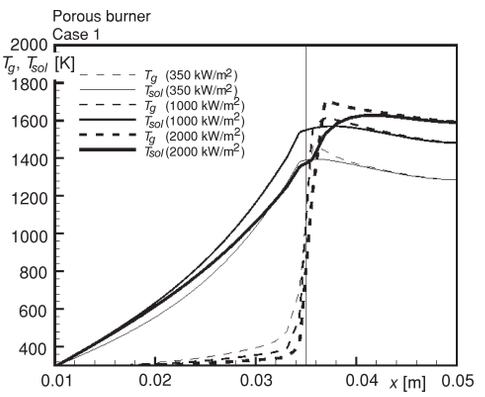

Figure 6. Temperature profiles for λ_2 effective conductivity of the Zone A

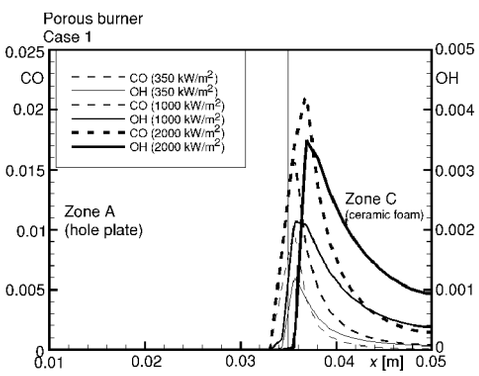

Figure 7. Mass fraction profiles of OH and CO for λ_2 effective conductivity of the Zone A

conductivity. The level of values of λ_1, λ_2, and λ_3 are shown in fig. 2. All calculations were accomplished with the same boundary conditions.

All temperature profiles have a form characteristic porous burner, with certain differences between the gas and the solid temperature. In the flame stabilization zone (Al_2O_3 hole plate) the solid temperature T_{sol} is much higher than the gas temperature T_g due to the higher conductivity of the solid. In this region the solid heats up the incoming gas. At the main reaction

zone (Zone C) it is the opposite. The heat source (combustion) is in the gas phase and so it heats up the solid. The peak temperatures of the gas phase is positioned just after the interface between the Al_2O_3 hole plate and porous combustion region (SiC foam). Convective heat transfer to the porous matrix and radiation losses of the later cause a decrease of the gas temperature in Zone C, while the solid temperature rises up slowly, reaching thermal equilibrium and following the gas temperature.

As it can be seen in figs. 3-6, the combustion temperature levels increase at higher power density. In addition, at higher power density the difference between gas and solid temperature at the peak gas temperature generally increases as well as its distance from interface between zones A and C. The peak temperature of the gas phase distance from the interface of zones A and C increases at higher power density because of the higher incoming gas velocities. Sharper gas temperature peak at higher power density results from the higher combustion heat source, whereby heat transfer between gas and solid matrix is not sufficiently high. However, the increasing the difference between gas and solid temperature at the peak, due to the power density increasing, is not linear. Moreover, maximum gas-solid temperature difference at power density of 350 kW/m^2 is even higher then at 1000 kW/m^2 (fig. 6). because the increasing of the power level implies two opposite effects: intensive combustion heat source and the increasing the gas mixture velocity, which results in the more intensive heat transfer between gas and solid matrix.

Regarding the influences of the Zone A heat conductivity properties on the temperature profiles, it can be seen that at the higher effective heat conductivities the temperatures are higher in Zone A and lower in Zone C, as the result of more intensive conductive heat transfer between zones A and C. Therefore, although the incoming gas mixture is more preheated in case of the higher Zone A effective heat conductivity, the temperatures in Zone C are lower then in case of the lower Zone A heat conductivity because of stronger influence of the effective heat transfer between A and C porous matrixes, that causes a cooling of the combustion zone.

The intensive combustion zone location, as well as the combustion efficiency can be analyzed using OH and CO profiles. It is well-known that the high concentration of OH is an indicator of the position of the main reaction zone. As it is shown in fig. 7 the position of the peak OH depends on the power density. This OH-peak dependence is the same as the peak gas temperature dependences (fig. 6.). The main combustion zone distance from the interface of zones A and C is downwind shifted at higher power density because of the higher incoming gas velocities, and consequently better cooling of the interface between zones A and C due to the incoming gas enthalpy. In addition, the combustion zone was more intensive cooling at higher gas velocities because of the porous matrix effective heat conductivity increasing due to its velocity dependence by the micro-convective term, eq. (12).

Zones of the intensive CO production correspond to the main reaction zones, as it can be seen from fig. 7. The same peak shifting effect occurs as in the case of the temperature profiles, which could cause the necessity of the longer combustion zone, due to the relatively high exit CO concentration at the higher combustion powers.

The surface burner (Case 2) temperature profiles of the solid and gas phase for different power densities and different porous matrix effective heat conductivities are

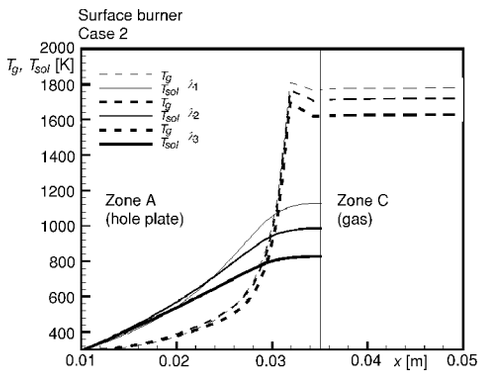

Figure 8. Temperature profiles at power density of 100 kW/m^2

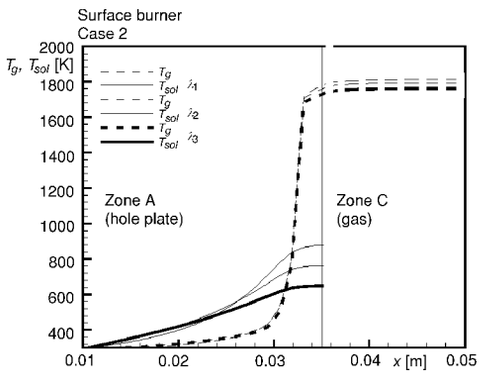

Figure 9. Temperature profiles at power density of 200 kW/m^2

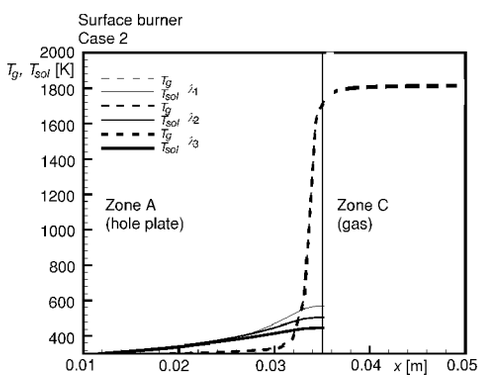

Figure 10. Temperature profiles at power density of 300 kW/m^2

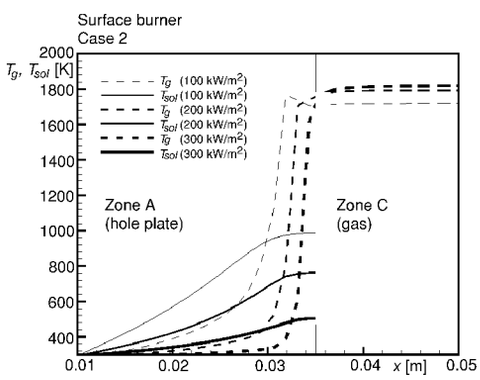

Figure 11. Temperature profiles for λ_2 effective conductivity of the Zone A

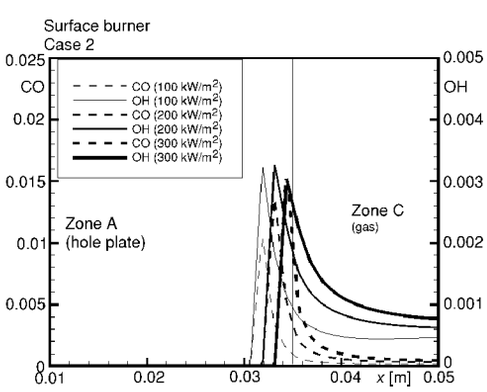

Figure 12. Mass fraction profiles of OH and CO for λ_2 effective conductivity of the Zone A

shown in figs. 8-11. The combustion temperatures are significantly higher then in the Case 2 in spite of lower power densities, as the result of a less intensive heat transfer from the combustion zone (Zone C). The combustion zone in case of the surface burner is without porous matrix. This means less intensive heat transfer by the conduction and radiation from Zone C. In case of the present surface burner higher power densities are not possible due to the flame blow off effects. The high combustion temperatures provide suitable

conditions for more intensive NO_x production.

As it is in the Case 1 there are significant differences between the solid and gas temperatures too, but in the Case 2 the solid temperatures in the Zone A (Al_2O_3 hole plate) are lower then in the case of porous burner. This is due to the less intensive heat transfer from the combustion zone to the flame stabilization zone in the case of the surface burner. The gas temperatures in the Zone A are higher then in the case of the porous burner, because the main combustion zones are placed very close to the hole plate surface. Moreover, at less power densities the intensive combustion is located even inside of the Zone A, as it can be seen from OH profiles in fig. 12.

The influences of the Zone A effective heat conductivities are more significant at lower power densities (figs. 8-10), due to the less influence of the convective heat transfer in comparison to the hole plate effective conduction. All temperatures are higher at lower effective heat conductivities due to the less temperature lose whereby the main combustion zone is located at the end of the Zone A.

Conclusions

A concept of the numerical simulation of complex processes in the porous and surface burners is proposed. For the porous regions the momentum and energy equations have appropriate corrections. The model describes separately gas and solid phase heat transfer, as well as heat transfer between gas and solid matrix. The radiation heat transfer is modeled separately for heat transfer within the porous matrix and between the solid phase and the environment. The radiation heat transfer within the porous matrix was included in the effective heat conductivity coefficients of the porous medium.

The proposed numerical tool is applied for the analyses of the combustion and heat transfer processes which take place in porous and surface burners. The numerical experiments are accomplished for different powers of the porous and surface burners, as well as for different heat conductivity characteristics of the porous regions.

All numerical simulations show certain differences between the gas and the solid temperature in Zone A. In the case of the porous burner (Case 1) the solid temperature is much higher than the gas temperature due to the higher conductivity of the solid, but in the case of the surface burner (Case 2) the gas temperatures in the Zone A are higher, due to the less intensive heat transfer from the combustion zone to the flame stabilization zone. In addition the combustion zones are placed very close to the hole plate surface. Generally, the combustion temperatures in Case 1 are significantly higher then in the Case 2 in spite of the lower power densities, due to the less intensive heat transfer from the combustion zone. The combustion zone in the case of the surface burner is without porous matrix, which less intensive heat transfer by the conduction and the radiation from Zone C. The high combustion temperatures provide suitable conditions for more intensive NO_x production. Besides, in the case of the surface burners higher power densities are not possible due to the flame blow off effects. This confirms obvious advantages of the porous burner concept.

In the case of the surface burner the peak temperatures of the gas phase is positioned just after the interface between the Al_2O_3 hole plate and porous combustion region and corresponds to the main combustion zone, which is confirmed through the analyze of the OH profiles. At the higher power density at the peak gas temperature the difference between gas and solid temperature generally increases, as well as its distance from interface between zones A and C. Zones of the intensive CO production correspond to the main reaction zones, and the same peak shifting effect occurs. This could cause the necessity for the longer combustion zone to avoid the relatively high exit CO concentration at higher combustion powers.

The influences of the Zone A effective heat conductivities are more significant at lower power densities due to the less influence of the convective heat transfer in comparison to the hole plate effective conduction. In the Case 2 the combustion temperatures are higher at lower effective heat conductivities due to the less temperature lose. This temperature increasing is especially significant at the lower power density. Although the incoming gas mixture is more preheated for the higher Zone A effective heat conductivity in the Case 1, the temperatures in Zone C are lower then in the case of lower hole plate heat conductivity, due to the cooling of the combustion zone by the more intensive effective heat transfer between A and C porous matrixes.

Acknowledgment

The paper is accomplished within the scope of the cooperation between the Institute of Fluid Mechanics (LSTM) in Erlangen and the Laboratory for Thermal Engineering and Energy of the VINČA Institute of Nuclear Sciences in Belgrade. For this fruitful and intensive cooperation Prof. Franz Durst, Head of LSTM, is gratefully acknowledged.

Nomenclature

A – surface, m^2
– atomic weight, –
A_V – specific surface, m^2/m^3
a – radiation emissivity, –
C_B – Stefan-Boltzman constant, –
c_p – fluid heat capacity for constant pressure, J/kgK
c – molar concentrationa, mol/m^3
D – mass diffusion coefficient, m^2/s
d – characteristic length of the porous media, m
E – activation energy, J/mol
h – enthalphy, J/kg
H – heat formation, J/kg
K_1 – permeability for laminar flow, m^2
K_2 – permeability for turbulent flow, m
K_C – chemical equilibrium constant, –
k – heat dispersion coefficients, –
– reaction rate constant, l/s

k_l^0 – collision-frequency factor, l/s
M – molar mass, kg/mol
$\dot{m}/A$ – mass flux, kg/sm^2
N_S – number of species, –
p – pressure, Pa
Q_R – radiation heat transfer between solid and environment, W/m^3
R – universal gas constant, J/mol·K
R_k – chemical conversion rate, kg/sm^3
S_ϕ – sources and sinks of ϕ, in arbitrary units
T – temperature, K
U – velocity vector, m/s
x – axial coordinate and distance, m
Y – mass fraction, –

Greek symbols

α – gas-solid heat transfer coefficient, W/m·K
Γ – diffusion coefficient, m^2/s
Δl – caracteristic length, m
ε – porosity, –
λ – heat conductivity, W/m^{2}K
μ – dynamic viscosity, Pa·s
ν – stoichiometric number, mole number, –
ρ – density, kg/m^3
ϕ – general variable, in arbitrary units
ψ – extinction coefficient, 1/m

Subscripts

eff – effective
g – gas
i, j – 2D directions
k – chemical species
l – chemical reactions
s, sol – solid
0 – environment
– without flow

Superscripts

a – temperature exponent

References

[1] Stone, H. L., *SIAM J. Num. Anal.*, *5* (1968), pp. 530-558
[2] Patankar, S. V., Spalding, D. B., *Int. J. Heat Mass Transfer*, *15* (1972), pp. 1787-1906
[3] Kee, R. J., Rupley, F. M., Miller, J. A., The Chemkin Thermodynamic Data Base, Sandia National Laboratories Rept. SAND-8215B, 1992

[4] Decker, S., Mößbauer, S., Nemoda, S., Trimis, D., Zapf, T., Detailed Experimental Characterization and Numerical Modelling of Heat and Mass Transport Properties of Highly Porous Media for Solar Receivers and Porous Burners, *Proceedings,* 6th International Conference on Technologies and Combustion for a Clean Enviroment, July 2001, Porto, Vol II, pp. 699-706
[5] Mishra, S. C., Steven, M., Nemoda, S., Talukdar, P., Trimis, D., Durst, F., Detailed Heat Transfer Analysis of a Two-Dimensional Rectangular Porous Radiant Burner, *Proceedings*, 7th International Conference on Energy for a Clean Environment (Clean Air 2003), July 2003, Lisbon, Portugal
[6] Kazakov, A., Frenklach, M., Reduced Reaction Sets Based on GRI-Mech 1.2. University of California at Berkeley, USA, 1994

Author's addresses:

S. Nemoda, G. Živković
Laboratory for Thermal Engineering and Energy,
VINČA Institute of Nuclear Sciences
P. O. Box 522, 11001 Belgrade, Serbia and Montenegro

D. Trimis
Institute of Fluid Mechanics (LSTM),
Technical Faculty
Friedrich-Alexander University, Erlangen-Nuremberg
Cauerstrasse 4, D-91058 Erlangen, Germany

Corresponding author (S. Nemoda):
E-mail: snemoda@vin.bg.ac.yu

Paper submited: February 5, 2004
Paper revised: March 15, 2004
Paper accepted: March 22, 2004